



HAL
open science

Thermodynamical effects of ocean current feedback in a quasi-geostrophic coupled model

Quentin Jamet, Alexandre Berger, Bruno Deremble, Thierry Penduff

► To cite this version:

Quentin Jamet, Alexandre Berger, Bruno Deremble, Thierry Penduff. Thermodynamical effects of ocean current feedback in a quasi-geostrophic coupled model. *Journal of Physical Oceanography*, 2024, pp.1-33. 10.1175/JPO-D-23-0159.1 . hal-04606538

HAL Id: hal-04606538

<https://hal.science/hal-04606538>

Submitted on 10 Jun 2024

HAL is a multi-disciplinary open access archive for the deposit and dissemination of scientific research documents, whether they are published or not. The documents may come from teaching and research institutions in France or abroad, or from public or private research centers.

L'archive ouverte pluridisciplinaire **HAL**, est destinée au dépôt et à la diffusion de documents scientifiques de niveau recherche, publiés ou non, émanant des établissements d'enseignement et de recherche français ou étrangers, des laboratoires publics ou privés.



Distributed under a Creative Commons Attribution 4.0 International License

1 **Thermodynamical effects of ocean current feedback in a quasi-geostrophic**
2 **coupled model**

3 Quentin Jamet,^a Alexandre Berger,^b Bruno Deremble,^b Thierry Penduff,^b

4 ^a *INRIA, ODYSSEY group, Ifremer, Plouzané, France*

5 ^b *Univ. Grenoble Alpes, CNRS, IRD, Grenoble INP, IGE, Grenoble, France*

6 *Corresponding author: Quentin Jamet, quentin.jamet@inria.fr*

7 ABSTRACT: Air-sea fluxes are the main drivers of ocean circulation, yet their representation in
8 ocean only models remains challenging. While a zeroth-order formulation accounting only for
9 the state of the atmosphere is well adopted by the community, surface ocean feedback has gained
10 attention over the last decades. In this paper, we focus on thermodynamical indirect feedback
11 of surface ocean currents, which completes the '*eddy killing*' effect induced by the mechanical
12 feedback. In this study, we quantify both the mechanical and thermodynamical contributions in
13 the context of idealized, coupled Quasi-Geostrophic simulations through sensitivity experiments
14 on wind stress formulation. As compared to *eddy killing* which impacts kinetic energy levels,
15 the indirect thermodynamical feedback induces significant changes in potential energy levels.
16 The thermodynamical feedback also enhances by +27% the potential-to-kinetic turbulent energy
17 conversion induced by relative wind stress formulation, as well as significant changes in both
18 forward and inverse cascades of Potential Energy (PE). That is, accounting for ocean surface
19 currents in the computation of wind stress significantly changes transfers of PE from the mean to
20 the turbulent flow. These changes are mostly controlled by a reduced upscale energy flux rather
21 than a more vigorous downscale flux, a process in line with results obtained for kinetic energy
22 fluxes associated with the *eddy killing* effect.

23 1. Introduction

24 The large-scale oceanic circulations is in constant interaction with 'eddies', the macro-turbulent
25 structures that develop in response to large-scale flow instabilities (McCaffrey et al. 2015). It is
26 now widely recognized that eddies feed back part of their energy upscale, and ultimately contribute
27 in shaping large-scale oceanic currents (Deremble et al. 2023). This has motivated intensive
28 work in the development of efficient/robust parameterizations of eddy-mean flow interactions for
29 climate models. Most of our knowledge on these interactions is based on studies investigating
30 these questions in the context of ocean-only simulations (e.g. Waterman and Jayne 2011; Kang
31 and Curchitser 2015). However, air-sea interactions have the potential to modulate both the mean
32 flow and the eddy field (Renault et al. 2016), hence their interactions.

33 In this paper, we are interested in quantifying the effects of dynamical and thermodynamical
34 ocean-atmosphere coupling on the energetics of the mean flow and eddy flow. Our first focus
35 is to quantify the impact of relative wind *vs.* absolute wind formulation of the ocean surface
36 stress, one of the well known mesoscale air-sea interaction processes (see Seo et al. 2023, for
37 a recent review). Dewar and Flierl (1987) and Pacanowski (1987) were among the first to show
38 the significant contribution of momentum air-sea feedback for the ocean energetics. In its *relative*
39 version, the magnitude of wind stress is proportional to the square of the difference between
40 atmospheric winds and ocean surface currents:

$$\tau_{rel} = \rho_a C_D |\mathbf{u}_a - \mathbf{u}_o| (\mathbf{u}_a - \mathbf{u}_o), \quad (1)$$

41 with ρ_a the density of air at sea level, C_D the drag coefficient, \mathbf{u}_a the atmospheric wind at the
42 surface of the ocean and \mathbf{u}_o the ocean surface currents. In the development of ocean models, the
43 wind stress was often formulated in its absolute version, i.e.

$$\tau_{abs} = \rho_a C_D |\mathbf{u}_a| \mathbf{u}_a, \quad (2)$$

44 which is a zeroth-order approximation of air-sea momentum coupling assuming much larger surface
45 winds ($\mathcal{O}(10 \text{ m s}^{-1})$) as compared to ocean surface currents ($\mathcal{O}(0.1 \text{ m s}^{-1})$). However, formulating
46 the wind stress with Eq. (1) or Eq. (2) can have drastic consequences on the ocean circulation.

47 Indeed, in the Ekman layer, the convergence of the Ekman transport results in an Ekman pumping
48 (vertical velocity from the Ekman layer toward the ocean interior) or Ekman suction (vertical
49 velocity from the ocean interior toward the Ekman Layer). This vertical velocity is often computed
50 as

$$w_{ek} = \mathbf{k} \cdot \frac{\nabla \times \boldsymbol{\tau}}{f_0} \quad (3)$$

51 with $\boldsymbol{\tau}$ the surface stress either computed following Eq. (2) or Eq. (1).

52 As noted in Gaube et al. (2015), when computed with relative wind, one can decompose this
53 Ekman pumping into a large-scale component and a small-scale component. The large-scale
54 component is mostly due to the large-scale winds and can be considered as a forcing which results
55 in the formation of large-scale oceanic gyres. On the other hand, the small scale component is
56 correlated with the presence of oceanic eddies and acts in two ways:

- 57 • First, the small-scale Ekman pumping induces a drag at the surface of the ocean and thus
58 extracts surface ocean kinetic energy. This can be shown analytically by calculating the change
59 in wind work (i.e. the mechanical energy input from the atmosphere to the ocean) induced
60 by ocean surface currents feedback, and highlighting its negative definite contribution (see
61 Appendix D). Scaling arguments and numerical investigations (Dawe and Thompson 2006;
62 Duhaut and Straub 2006; Song et al. 2020; Jullien et al. 2020, among others) suggest a
63 reduction of the order of 20% to 40% on basin averaged estimates, with important regional
64 variations depending on eddy activity.

65 Renault et al. (2016) identified two main impacts of this *eddy killing* effect for the energetics
66 of the North Atlantic subtropical gyre. First, through a reduced wind work in the tropics,
67 the energy injected by the atmosphere into the ocean is reduced by about 30%. Jamet et al.
68 (2021) also showed that the mean Kinetic Energy (KE) of the Gulf Stream is then reduced
69 in response to a non-local inertial recirculation toward the western boundary dynamics. The
70 Gulf Stream is then more stable and less prone to eddy generation. A second local impact
71 of relative wind stress is to extract surface kinetic energy of ocean eddies downstream of the
72 Gulf Stream separation, with a 27% reduction of the depth integrated Eddy Kinetic Energy
73 (EKE) (Renault et al. 2016).

- Another effect that has not received a lot of attention is the thermodynamical consequences of this Ekman pumping. Indeed, the vertical velocity transports heat either from the mixed layer to the ocean interior or from the ocean interior to the mixed layer. For a well defined eddy, this transport will always remove heat anomalies, damping the eddy (Gaube et al. 2015), thus its associated Available Potential Energy (APE). When accounting for ocean surface currents in wind stress formulation, eddies are thus damped by both mechanical (eddy killing) and thermodynamical (Ekman pumping) effects.

The main objective of this paper is to quantify and interpret the thermodynamical feedback for the ocean energy cycle in the context of idealized, coupled quasi-geostrophic simulations. The paper is organized in the following way. In Section 2, we first introduce the Q-GCM model of Hogg et al. (2006) that we use for two simulations: one run with an absolute wind stress formulation following Eq. (2), and another run with a relative wind stress formulation following Eq. (1). In Section 3, we quantify and discuss the wind stress contribution in these two simulations for both the kinetic and potential energy of the eddy field. As will be shown, the main effect of using a relative wind stress formulation is to change the turbulent wind work and turbulent diabatic heating forcing from sources to sinks of (kinetic and potential, respectively) energy, on average. Although the mechanical contribution of relative wind stress for EKE is not new, its thermodynamical contribution for Eddy Potential Energy (EPE) has not received a lot of attention. In Section 4 we analyze the consequence of the thermodynamical feedback for the energy transfers between different energy reservoirs, namely the Mean KE, Eddy KE, Mean PE and Eddy PE, using the Lorenz Energy Cycle (LEC; Lorenz 1955; Harrison and Robinson 1978; Oort et al. 1994; Matsuta and Masumoto 2023) framework. We will pay a particular attention to the eddy potential-to-kinetic energy conversion as well as to the eddy-mean flow potential energy transfers. Still in Section 4, we also quantify and discuss the non-locality associated with eddy-mean flow interactions, a characteristic that has been recently highlighted in several studies (e.g. Murakami 2011; Chen et al. 2014; Kang and Curchitser 2015; Matsuta and Masumoto 2021; Jamet et al. 2022), and which is critical in order to interpret the spatial organization of eddy-mean flow energy transfers. We end this paper with a summary of main results and conclude on the extension of these results in the context of realistic modelling in Section 5.

103 2. Methods

104 a. The Quasi-Geostrophic Coupled Model (Q-GCM)

105 In this study, we investigate the exchanges of energy between the (temporal) mean and turbulent
 106 flow in an idealized, numerical framework. We use the Quasi-Geostrophic Coupled Model (Q-
 107 GCM Hogg et al. 2006). This idealized coupled ocean-atmosphere model is meant to represent
 108 the dynamics of extratropical climate. It solves the Quasi-Geostrophic Potential Vorticity (QGPV)
 109 equation in both the ocean and the atmosphere, and boundary layers are used to couple the system.
 110 The coupling involves Ekman dynamics, entrainment and thermal exchanges. An additional Ekman
 111 layer is included in the bottom layer of the ocean, and lateral limits are treated as solid boundaries
 112 with mixed no-slip/free-slip conditions, expressed on pressure gradients (see Hogg et al. 2006, for
 113 details).

114 The setup is very similar to Martin et al. (2020). The (zonally periodic) atmosphere is horizontally
 115 discretized on 384×96 grid cells (64 km resolution), and the ocean on 1024×1024 grid cells (5 km
 116 resolution) for a square ocean basin dimension of 5120×5120 km. Both fluids are vertically
 117 discretized with 3 layers, the total depth of the ocean is 4 km, and 10 km for the atmosphere Upper
 118 (bottom) ocean Ekman layer thickness is set to 100 m (5 m),

119 Following Hogg et al. (2014) and Martin et al. (2020), the Quasi-Geostrophic vorticity equation
 120 solved by Q-GCM can be expressed in the following compact, vector form (we only recall the
 121 equations for the ocean):

$$\partial_t \mathbf{q} = \frac{1}{f_0} J(\mathbf{q}, \mathbf{p}) + \underline{\underline{\mathbf{B}}} \mathbf{e} - \frac{\mathcal{A}_4}{f_0} \nabla_H^6 \mathbf{p}, \quad (4)$$

122 with

$$\mathbf{q} = \beta(y - y_0) + \frac{1}{f_0} \nabla^2 \mathbf{p} - f_0 \underline{\underline{\mathbf{A}}} \mathbf{p}, \quad (5)$$

123 where $\mathbf{p} = (p_1, p_2, p_3)$ and $\mathbf{q} = (q_1, q_2, q_3)$ represent the pressure and the QGPV in layers 1 to
 124 3, $J(A, B) = \partial_x A \partial_y B - \partial_x B \partial_y A$ is the Jacobian operator, and $\mathcal{A}_4 = 2 \times 10^9 \text{m}^2 \text{s}^{-1}$ is the constant
 125 biharmonic viscosity. $\underline{\underline{\mathbf{A}}}$ is a 3×3 matrix containing the coefficients of the pressures in the η
 126 contribution to vorticity, and $\underline{\underline{\mathbf{B}}}$ is a 3×4 matrix containing the inverse layer thicknesses. Finally, \mathbf{e}
 127 is the entrainment vector which couples the atmospheric Ekman layer, the oceanic surface Ekman
 128 layer and the oceanic bottom Ekman layer to the 3 layers of the QG model. It is expressed as follow

129 (for the ocean):

$$e = \begin{bmatrix} w_{ek} \\ -\frac{T_m - T_1}{2(T_1 - T_2)} w_{ek} \\ 0 \\ \frac{\delta_{ek}}{2f_0} \nabla^2 p_3 \end{bmatrix} \quad (6)$$

130 with w_{ek} the Ekman pumping defined in Eq. (3), T_m the temperature in the surface mixed layer and
 131 T_1 (T_2) the temperature in the first (second) QG layer.

132 The temperature difference between 2 layers and vertical Ekman pumping determine the entrain-
 133 ment heat flux. In our model, the layer's temperature is considered constant and only the mixed
 134 layer's temperature is time-dependant and inhomogeneous. Vertical heat fluxes which result in the
 135 modification of the layer temperature in a specific area are handled through layer stretching: the
 136 interface with the upper/lower layer is elevated/lowered over the downwelling/upwelling area, thus
 137 locally changing the temperature. The entrainment heat term appearing in the potential vorticity
 138 equation is defined only at the interface between the first and second layer:

$$F_k^{th} = \pm \frac{f_0}{H_k} \frac{(T_m - T_1) w_{ek}}{T_1 - T_2} \quad (7)$$

139 with H_k the k^{th} layer thickness, this term is defined with a plus sign in the first layer potential
 140 vorticity equation and a minus sign in the second layer. The entertainment heat flux through the
 141 layer interface influences layer's temperatures according to the sign and amplitude of the vertical
 142 velocity. As discussed in introduction, surface current feedback will modify the curl of the wind
 143 stress, thus the induced Ekman pumping (Eq. (3)).

144 In order to highlight the impact of relative wind on the oceanic circulation, we run two config-
 145 urations of the model: one with absolute wind stress formulation following Eq. (2) (referred to as
 146 ABS hereafter), the other with relative wind stress formulation following Eq. (1) (referred to as
 147 REL hereafter). In both cases, the simulations are ran for 50 years after a common 80-year spin-up,
 148 and all the diagnostics are computed over the last 10 years. Although relatively short, the duration
 149 of the simulation is sufficient for the model to achieve a quasi-steady state (cf Fig. 4 of Martin
 150 et al. (2020)). The derivation of the LEC in QG is provided in Appendix A for completeness, and

151 some discussion on non-locality of eddy-mean flow energy transfers are provided in Appendix B.
152 Table A1 summarizes the different terms associated in the energy equations. Following Harrison
153 and Robinson (1978), we will refer to potential-to-kinetic energy exchange as energy *conversion*,
154 since the term responsible for it (i.e. wb) is mathematically identical in both kinetic and potential
155 energy equations but with an opposite sign. However, the terms responsible for eddy-mean flow
156 energy exchange are not identical in the eddy and in the mean equations, where significant non-
157 local contributions can be involved when considered regionally (see Appendix B). To highlight
158 this difference, we will refer to this type of energy exchange as energy *transfer*, which formally
159 represents the energetic signature of eddy-mean flow interactions. In keeping with notation in
160 Jamet et al. (2022), we will use the shorthand 'MEC' to refer to the terms associated with the mean
161 equations, and the shorthand 'EF' to refer to the terms associated with the eddy equations. For
162 the potential energy equations, these terms will read P_MEC and P_EF, respectively, and for the
163 kinetic energy equations, they will read K_MEC and K_EF. We will also perform wavenumber
164 spectral analysis of relevant terms in order to assess the energy distribution and fluxes as a function
165 of spatial scale. Details are provided in Appendix C (also see, e.g. Capet et al. 2008a; Arbic et al.
166 2013, for consistency). We simply recall here that a positive (negative) slope in spectral fluxes is
167 associated with a sink (source) of energy within the associated waveband, and that the basin scale
168 estimate (smallest wavenumber) reflects the values reported in the LEC (Fig. 1).

169 **3. Mechanical and thermodynamical ocean surface fluxes**

170 Fig. 1 synthesizes the content of the four energy reservoirs along with the associated exchanges,
171 and the forcing and dissipative energy fluxes for the two simulations ABS and REL. Absolute
172 values are given for ABS and relative differences observed in REL are expressed in % (see caption
173 for details). In both cases, the external forcing terms responsible for energy exchanges with the
174 atmosphere are the diabatic heating and the wind stress forcing (top and bottom arrows), driving
175 potential and kinetic energy, respectively. Bottom friction and viscous dissipation represent the
176 internal processes resulting in a drain of Kinetic Energy (right arrows).

177 This diagram exhibits the hierarchy between energy reservoirs traditionally diagnosed in geo-
178 physical flows (Vallis 2006): the Mean Potential Energy (MPE) level is the largest, then comes
179 the EKE, the EPE, and the Mean Kinetic Energy (MKE). More than 80% of the total energy of

180 the ocean is stored in the potential energy of the mean flow. This means that nearly all of the
181 mean ocean energy is present as buoyancy anomaly (potential energy) rather than transport (kinetic
182 energy). For the eddy field, there is roughly an equipartition between EKE and EPE, as expected
183 from QG theory.

184 Comparing ABS and REL first reveals that the most important contribution of relative wind
185 stress formulation is to change the sign of turbulent wind work and turbulent diabatic heating
186 (i.e. turbulent surface forcing; bottom black and red arrows). In the ABS simulation (numbers in
187 black), the turbulent wind work provides energy to the EKE at a rate of +3 GW and the turbulent
188 diabatic heating provides energy to the EPE at a rate of +1 GW. In contrast in the REL simulation
189 (numbers in blue), the turbulent wind work extracts energy from the EKE at a rate of -11 GW
190 and the turbulent diabatic heating extracts energy from the EPE at a rate of -5 GW. The global
191 energy balance is also significantly modified, with a reduction of about 20% in energy input and
192 dissipation. The relative contributions of turbulent wind work and turbulent diabatic heating to the
193 total energy balance thus jump from 4% and 1% in ABS, respectively, to 19% and 9% in REL, in
194 agreement with recent estimates (Zhu et al. 2023). The wind stress formulation thus has two main
195 contributions in how the ocean and the atmosphere components of the Q-GCM interact through
196 eddies.

197 First, the relative wind stress formulation strongly increases the relative contribution of both
198 air-sea turbulent fluxes by about one order of magnitude in the global energy balance, a result
199 of both a reduced total energy balance and a significant amplification of the turbulent wind work
200 and turbulent diabatic heating. Second, the relative wind stress formulation reverts surface eddy
201 fluxes from a source to a sink of eddy energy. The contribution of these turbulent fluxes are mostly
202 confined within the jet region (Fig. 2), where most of ocean turbulence is observed. Turbulent
203 wind work is characterized by positively skewed eddy-size structures in ABS, leading to a net
204 positive contribution (i.e. a source of EKE) over the full domain. This eddying structure changes
205 radically into a broad and homogeneous negative structure (i.e. a sink of EKE) along the jet in
206 REL, with residual positive contributions in the ocean interior. Such a change is consistent with
207 the *eddy killing* effects observed by Renault et al. (2016) in their realistic simulations of the North
208 Atlantic simulations (cf their Figure 7). Similar results are found for the turbulent diabatic heating
209 (Fig. 2, bottom panels), which is also characterized by positively skewed eddy-size structures in

210 ABS (i.e. a source of EPE), but by an homogeneous negative contribution in REL (i.e. a sink of
211 EPE). The contribution of relative wind formulation on turbulent diabatic heating is to induce a
212 turbulent Ekman pumping driving heat flux between the Ekman layer and the upper QG layer. As
213 sketched on Fig. 3, cyclonic eddies are associated with a downwelling at the base of the Ekman
214 layer, inducing a downward heat flux within the upper layer T_1 , thus damping the negative heat
215 anomaly associated with cyclonic eddies. The opposite is true for anticyclonic eddies, where
216 relative wind stress induces an additional upwelling, extracting part of their positive heat anomaly.
217 For a well defined eddy, this transport will always reduce heat anomalies, damping the eddy, thus
218 its associated potential energy.

219 Turbulent diabatic heating can be further decomposed into a contribution associated with time
220 mean and time varying mixed layer temperature T_m (Fig. 4). This decomposition reveals turbulent
221 diabatic heating is largely driven by turbulent Ekman pumping acting on the time mean mixed
222 layer temperature, while the contribution of time variations of T_m plays a secondary, although
223 non-negligible, role. This result further supports our previous interpretation which neglects the
224 response of the oceanic mixed layer temperature to the induced heat fluxes associated with Ekman
225 pumping. We note, however, that in Q-GCM, air-sea heat fluxes are computed with a restoring
226 strategy, and do not account for relative wind stress formulation in these type of fluxes which may
227 well impact the temperature of the oceanic mixed layer. Further analyses would be required to
228 evaluate such a contribution for ocean energetics, but are outside of the scope the present paper.

229 Finally, we note that the budgets are not closed to machine precision, with sources and sinks
230 of total energy that do not perfectly balance, reflecting a rate of change of the different energy
231 reservoirs. These residuals are relatively weak (<10% for ABS and <5% for REL), and may
232 be due to the relatively short period used for the analysis (10 years) and to the relatively coarse
233 temporal resolution we used for saving model outputs (15-day averages). Another potential source
234 of uncertainty lies in eddy rectification term, which has been shown to converge very slowly
235 ($\sim O(10^4)$ years Uchida et al. 2022), contaminating the quality of the steady-state statistics.
236 However, we do not anticipate such convergence issue to significantly modify our estimates of the
237 time mean flow structure as the system reaches a nearly steady state after only 10 year of spin-up
238 (Martin et al. 2020). Especially, we have verified that the meridional extension of the oscillating
239 mean jet is a robust feature of the experiments, and does not reflect a transitional state induced by

240 a lack of convergence (not shown). This last point is of particular interest for the discussion in
 241 Section 4b, where we interpret the reduction of eddy-mean flow energy transfers in REL as a result
 242 of a more stable jet with less pronounced meanders. We do not expect such an interpretation to be
 243 biased by this potential convergence issue.

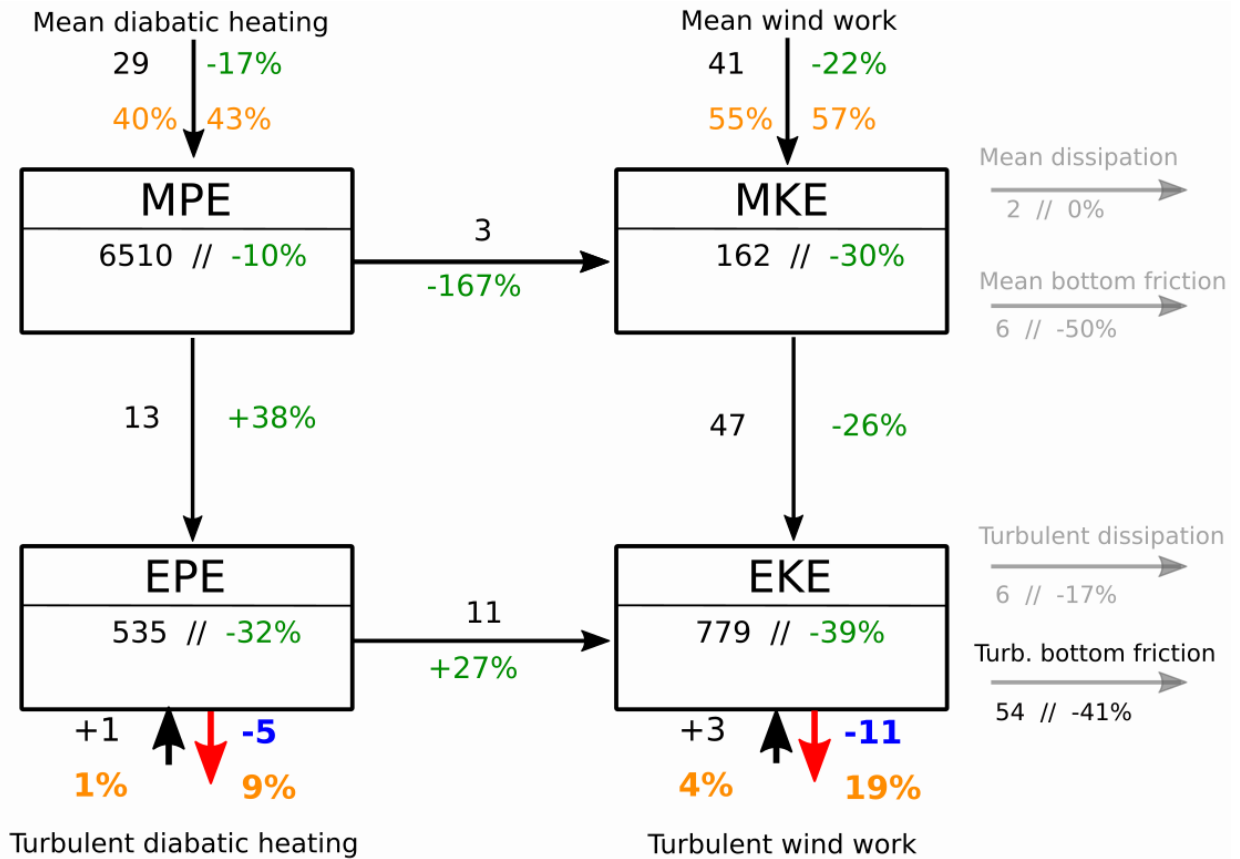


FIG. 1: Lorenz Energy Cycle for both simulations. Results for the absolute wind stress scenario (ABS) are shown in black, and the relative differences for the relative wind stress scenario (REL) are shown in green and expressed in %. For turbulent diabolic heating and wind work, energy fluxes for REL are reported in blue in order to highlight their changes in sign and magnitude. The relative contribution (in %) of wind work and diabolic heating for the total energy input/dissipation are also shown in orange. Units are in PJ (1 PJ = 10¹⁵ J) and GW (1 GW = 10⁹ W) for energy content and fluxes, respectively.

244 4. Energy exchanges

245 We now turn our attention to the modifications induced by a change from absolute to relative
 246 wind stress formulation for the exchanges between the different energy reservoirs. We focus here

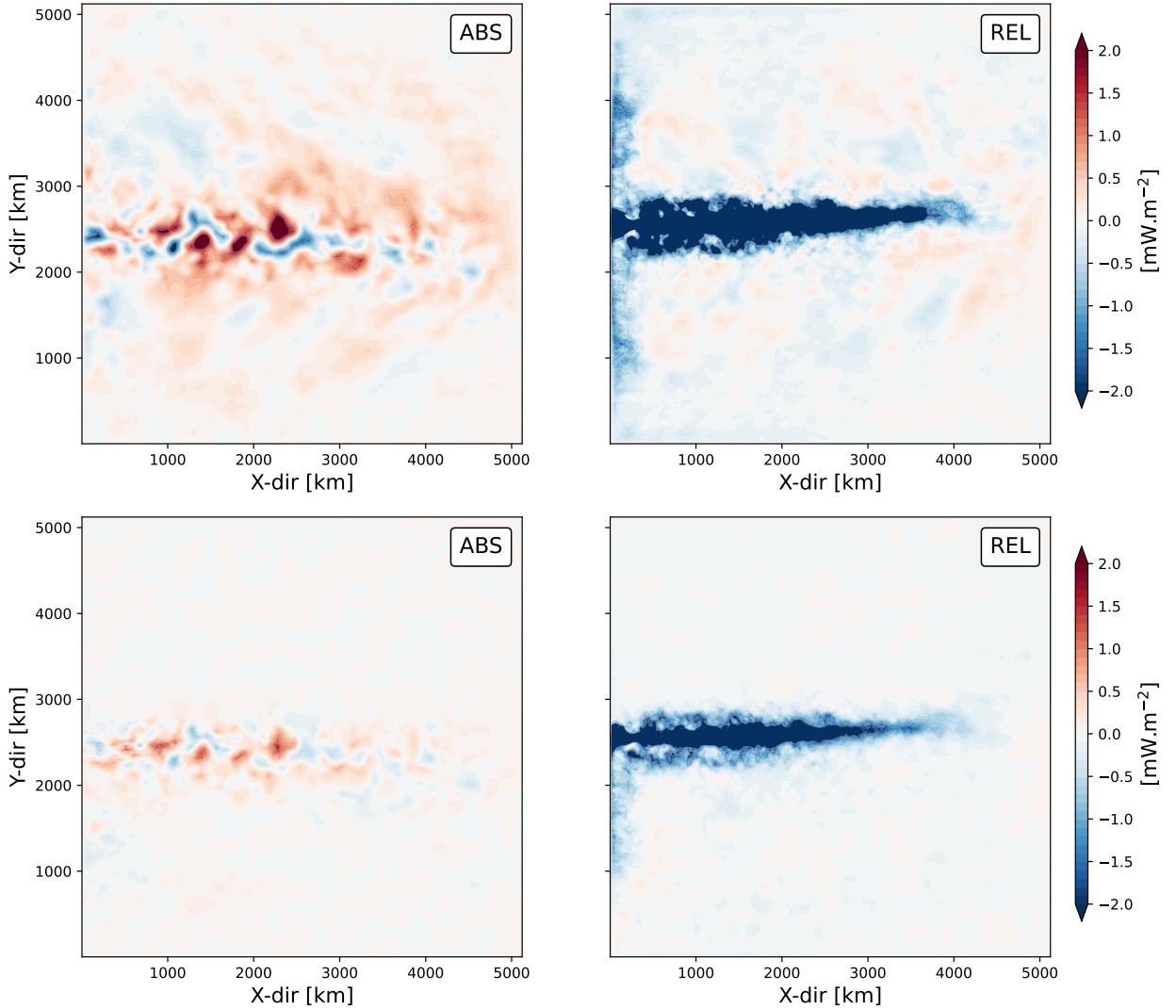


FIG. 2: (Top) Turbulent wind work, and (bottom) turbulent diabatic heating for the absolute (left) and the relative (right) simulation. (See text, Appendix A and Table A1 for further details of these terms).

247 on the potential-to-kinetic eddy energy conversion and on the eddy-mean flow potential energy
 248 transfers.

249 *a. Potential-to-kinetic eddy energy conversion*

250 As shown in Fig. 1, potential-to-kinetic eddy energy conversion (i.e. $\overline{w'b'}$) is +27% larger in
 251 REL. From the spatial distribution of energy conversion $\overline{w'b'}$ (Fig. 5), the net increase in energy
 252 conversion does not appear as an obvious signature, since both potential-to-kinetic (positive values)

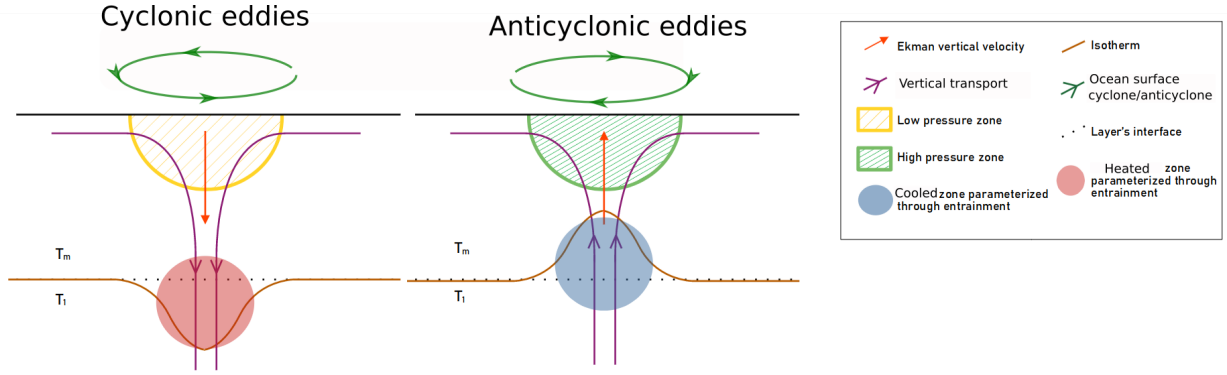


FIG. 3: Schematic of the process resulting in Ekman pumping, for cyclonic eddies (left) and anticyclonic eddies (right) in the Northern Hemisphere. T_m and T_1 refer to the temperature in the ocean surface mixed layer and in the ocean first QG layer, respectively.

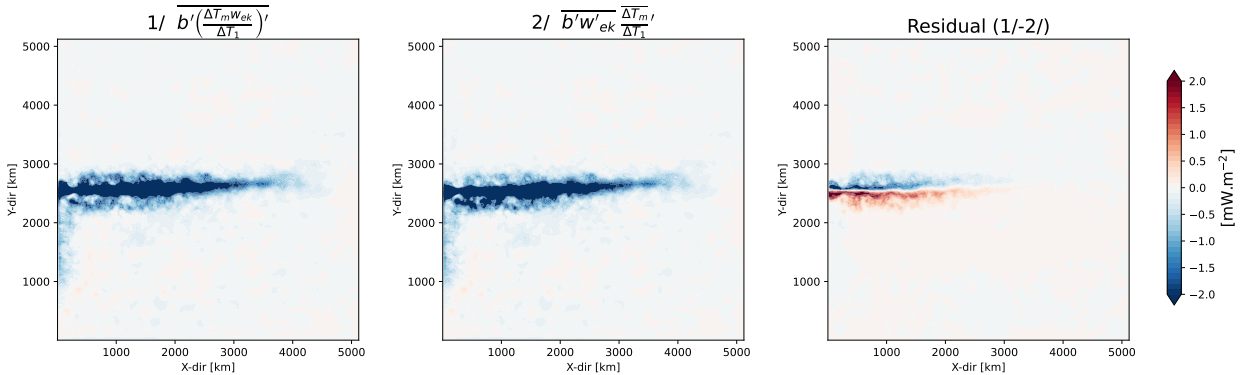


FIG. 4: Turbulent diabatic heating for REL (left), decomposed into a contribution driven by time mean mixed layer temperature T_m (centre) and T_m anomalies (computed as a residual ; right).

253 and kinetic-to-potential (negative values) energy conversion exhibit small differences between ABS
 254 and REL. It is their net, averaged effects that results in a +27% increase, indicative of a larger
 255 increase in potential-to-kinetic turbulent energy conversion. Spectral fluxes of energy between EPE
 256 and EKE (Fig. 5, bottom panel) provides a complementary view. We recover the net +27% at largest
 257 scale (smallest k), in agreement with the relative wind induced Ekman pumping anomaly due to
 258 absolute forcing (investigated by Gaube et al. 2015). However, the net increase is not uniformly
 259 distributed across scales, where we rather observe a significant reduction at most wavenumbers.
 260 That the net (basin scale estimates) spectral fluxes are larger in REL than in ABS is a consequence
 261 of a stronger reduction in EKE to EPE (positive slope) at low wavenumber than in EPE to EKE
 262 (negative slope) at high wavenumber. Thus, in the general energy cycle associated with baroclinic
 263 instability, where EPE is expected to be transferred toward EKE in order to be dissipated, this may

264 well suggest that relative wind stress favors scales associated with energy conversion needed to
 265 reach dissipative scales, thus an energetically balanced state.

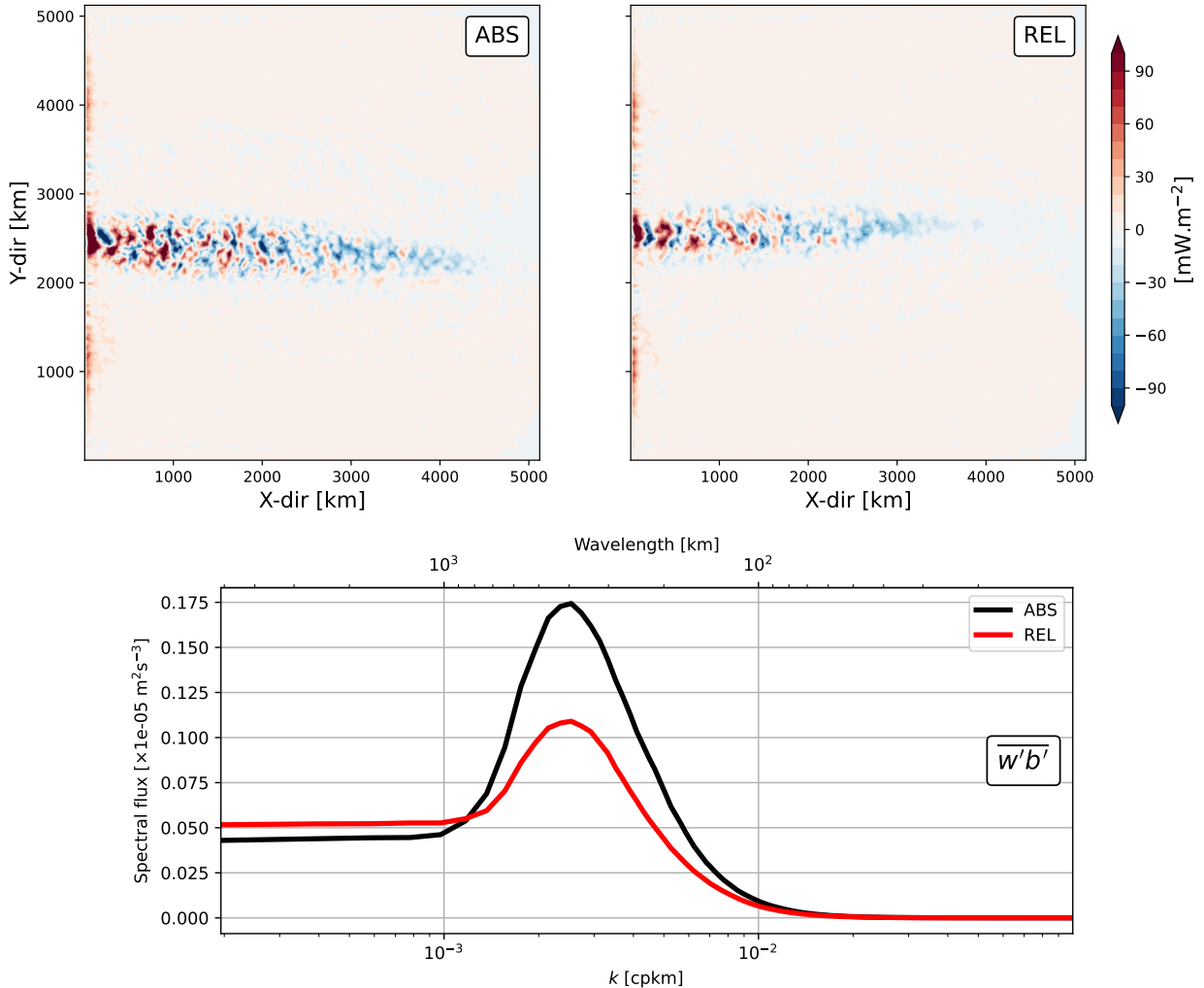


FIG. 5: (Top) Spatial distribution of energy conversion between the turbulent potential and turbulent kinetic energy ($\overline{w'b'}$) for the absolute (left) and the relative (right) simulation. Red (blue) regions are associated with a conversion from potential (kinetic) to kinetic (potential) turbulent energy. (Bottom) Spectral fluxes of energy conversion between the EPE and the EKE ($\overline{w'b'}$), where a positive slope is associated with a conversion from EKE to EPE and a negative slope is associated with a conversion from EPE to EKE. Net EPE-EKE conversion, as reported in Fig. 1, are associated with the value at the smallest k (i.e. left most values).

266 *b. Eddy-mean flow energy transfers*

267 Finally, we quantify the imprints of the relative wind stress formulation on the energy transfers
 268 between the mean and the turbulent flow. For KE, those transfers are usually related to barotropic

269 instabilities: Jamet et al. (2021) showed that at leading order in the Gulf Stream, this MKE to
270 EKE transfer roughly balances the net mean wind work over the North Atlantic subtropical gyre.
271 Here, we pay a particular attention to the eddy-mean flow transfers of potential energy as those
272 show a +38% increase in REL, which questions the underlying dynamics given both MPE and
273 EPE have decreased by -10% and -32% , respectively. In contrast, eddy-mean flow transfers of
274 kinetic energy are weakened by -26% , following the reduction of MKE and EKE of about the
275 same amplitude (cf Fig. 1) and consistent with Renault et al. (2019).

276 We show in Fig. 6 the spectral fluxes of P_MEC for ABS and REL. In both runs, spectral fluxes
277 reveal that MPE feeds EPE (i.e. positive slope) between 200 km and 1250 km ($k = 5 \cdot 10^{-3} - 8 \cdot 10^{-4}$
278 cpkm, respectively), a waveband corresponding to mesoscale turbulence suggesting mesoscale
279 eddy generation processes. This is a typical signature of a forward energy cascade. At larger
280 scales (1250 km - 2500 km ; $k = 8 - 4 \times 10^{-4}$ cpkm), spectral fluxes indicate a transfer from eddy
281 to mean potential energy (i.e. negative slope), indicative of a noticeable backscattering energy
282 contribution which is likely associated with the absorption of eddies by the mean flow. This is
283 a typical signature of an inverse energy cascade. By comparing the two simulations, it appears
284 that at nearly all scales shorter than 2500 km ($k > 4 \times 10^{-4}$ cpkm), P_MEC spectral fluxes are
285 weaker in REL than in ABS. Specifically, relative wind forcing yields a less vigorous forward
286 cascade at small scales (positive slopes for $k > 8 \times 10^{-4}$ cpkm), but more importantly, a very
287 strong reduction of the inverse cascade at scales between 1250-2500 km ($k = 8 - 4 \times 10^{-4}$ cpkm)
288 suggesting a significant weakening of the energy backscattering mechanism. A more pronounced
289 forward cascade completes the picture at basin scale in REL, which is responsible for the net +38%
290 increase of P_MEC reported in Fig. 1. Our results thus extend the recent results of Renault et al.
291 (2019) to potential energy. They observed a reduction of both forward and inverse cascades of
292 kinetic energy spectral fluxes in realistic coupled simulations of the Gulf Stream and the Agulhas
293 current, with a stronger reduction of the inverse cascade (30-40%) as compared to the reduction of
294 the forward cascade (10-20%).

295 To help our interpretation of the dynamics driving these eddy-mean flow potential energy trans-
296 fers, we show in Fig. 7 the depth integrated P_MEC contribution for which spectral fluxes have been
297 computed, as well as their EPE equivalent P_EF in Fig. 8. Indeed, to fully appreciate the spatial
298 organization of energy transfers between mean and turbulent energy reservoirs, it has recently been

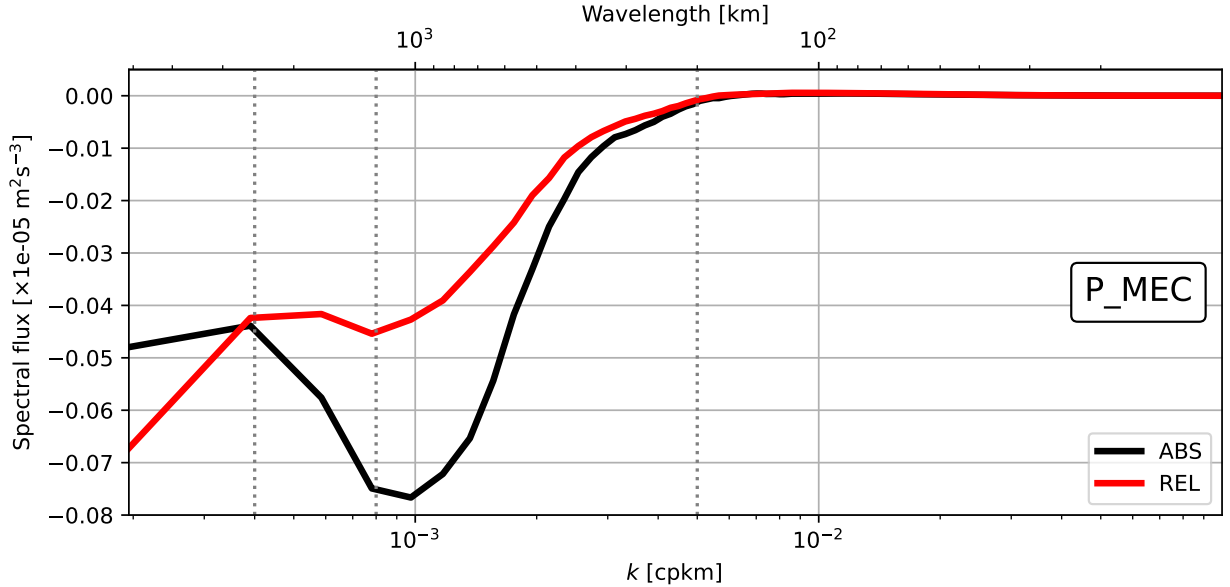


FIG. 6: Spectral fluxes of eddy-mean flow potential energy transfers (P_{MEC}). Positive slopes are associated with transfers from mean to eddy potential energy (i.e. forward cascade of energy), and negative slopes are associated with energy transfers from eddy to mean potential energy (i.e. inverse cascade of energy). Dotted vertical lines correspond to wavelength 2500 km, 1250 km and 200 km referred in the text.

299 shown by several studies that non-local energy transfers need to be considered (Chen et al. 2014;
 300 Kang and Curchitser 2015; Matsuta and Masumoto 2021; Jamet et al. 2022). Non-local processes
 301 reflect the fact that energy lost by the mean flow at one location can be transported over significant
 302 distances before to be either re-injected within the mean flow or sustain the growth of the turbulent
 303 flow. Formally, this can be explained through the divergence of a turbulent flux of cross energy
 304 terms (see Appendix B for further details). Comparing the spatial organization of P_{MEC} and
 305 P_{EF} (Fig. 7 and Fig. 8, respectively) provides a measure of such non-locality. Although in both
 306 ABS and REL differences are significant, we nonetheless point out that both P_{MEC} and P_{EF}
 307 exhibit some degree of spatial correlation between regions of negative P_{MEC} with regions of
 308 positive P_{EF} , as for example right at the western boundary where the jet detaches. The spatial
 309 organization of P_{MEC} and P_{EF} thus suggests non-local dynamics may not be a leading order
 310 contribution along the jet in our setup. This represents a noticeable difference with results from
 311 previous studies based on realistic, Primitive Equations models where non-locality has been found
 312 to be significant in eddy regions (i.e. western boundary currents, Antarctic Circumpolar Current ;
 313 e.g. Chen et al. 2014). Further analyses are required to evaluate if this is specific to our idealized

314 setting, or if it is a consequence expected under quasi-geostrophy. We still note one major differ-
315 ence between P_{MEC} and P_{EF} associated with their respective magnitudes along the jet: while
316 P_{EF} is maximum at the centre of the jet, P_{MEC} has a local minimum. This can be explained
317 by the dynamics behind these transfers: P_{EF} is associated with horizontal gradients of the mean
318 buoyancy field (i.e. $\nabla \bar{b}$), which are largest at the centre of the jet; on the other hand, P_{MEC} is
319 associated with mean buoyancy field \bar{b} , which is associated with a local minimum along the jet.
320 It is of interest to note that the spatial organization of P_{EF} share some similarities with K_{MEC}
321 (discussed in Jamet et al. 2022, but for Primitive Equations, realistic models), while the spatial
322 organization of P_{MEC} share some similarities with K_{EF} .

323 We now focus on the spatial organization of P_{EF} along the jet in ABS (Fig. 8, bottom left panel).
324 Comparing the meanders of the time mean jet, represented by the orange contour (cf caption), with
325 location of EPE sources and sinks, we can see that red (blue) regions are co-localized with the parts
326 of the meanders that move away (toward) the jet mean latitude (represented with a white line). The
327 spatial organization of P_{EF} with the meandering mean jet suggests preferred dynamical regions
328 for eddy generation (red spots) and eddy backscattering (blue spot) depending on the meridional
329 excursion of the mean jet. Given that the time mean jet in REL exhibits a much weaker meandering
330 structure (Fig. 8, bottom right panel), this may well provide a dynamical rationalization to interpret
331 the strong reduction of inverse energy cascade observed in REL. This statement, however, remains
332 speculative and is discussed here only to provide potential directions for further studies.

333 5. Conclusion and discussion

334 In this study, we have investigated the impact of the relative vs absolute wind stress formulation on
335 the ocean energy reservoirs and exchanges in the context of Lorenz Energy Cycles (LEC). We have
336 conducted this analysis with an idealized, coupled Quasi-Geostrophic model (Q-GCM Hogg et al.
337 2006), where a 3-layer QG ocean model interacts with a 3-layer QG atmospheric model through
338 Ekman layers. The main contribution of our study is to provide evidences of the thermodynamical
339 impact of ocean current feedback on the energetics of the ocean via Ekman pumping. Through
340 this effect, both up and down scale transfers of energy between mean and eddy potential energy,
341 as well as energy conversion between potential and kinetic energy of the eddies, are strongly
342 reduced. However, upscale transfers are more reduced than downscale transfers, resulting in a net

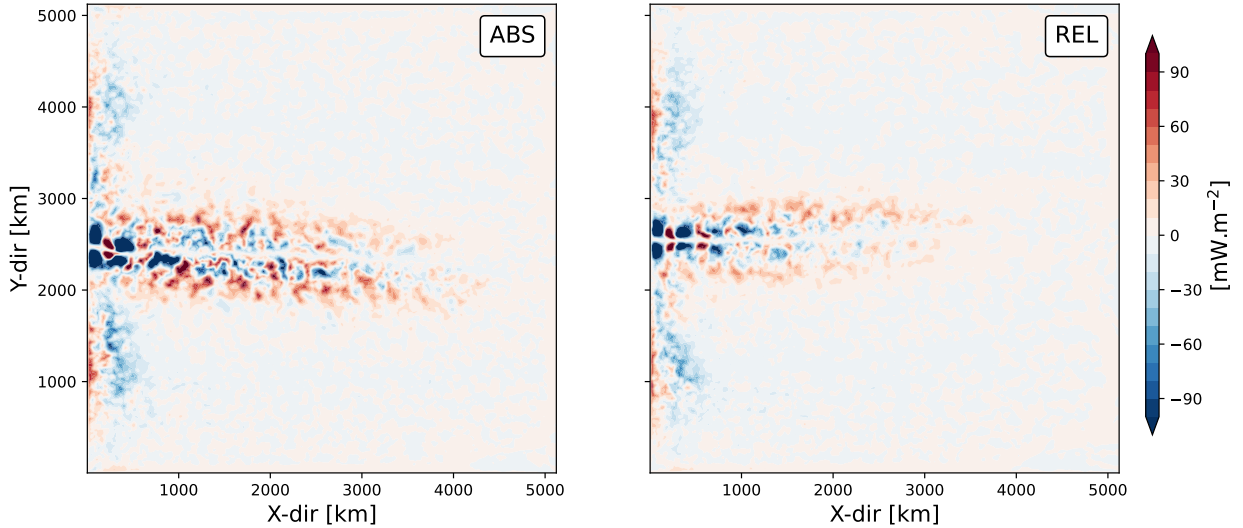


FIG. 7: Depth integrated contribution of P_{MEC} for the absolute wind stress (left) and for the relative wind stress (right) simulation. Red shading indicate a local source of MPE. The basin integrated contribution is a sink of MPE of about -13 (-18) GW for ABS (REL ; see Fig. 1)

343 increase of energy transfers (see Fig. 1). The reduced upscale transfer we observe in response to
 344 surface current feedback is consistent with what Renault et al. (2019) observed in realistic regional
 345 simulations and satellite observations in the Gulf Stream and the Agulhas current region for kinetic
 346 energy spectral fluxes. To our knowledge, spatial patterns and induced changes in energy transfers
 347 associated with the thermodynamical feedback have not been reported by others based on realistic
 348 simulations nor observations. Nonetheless, both mechanical (*eddy killing*) and thermodynamical
 349 (Ekman pumping) ocean current feedback have the expected behaviour on a basin averaged sense
 350 (Dewar and Flierl 1987; Gaube et al. 2015). We note that the relative impact of surface current
 351 feedback we have reported on here are to be interpreted cautiously for applications to realistic ocean
 352 models or observations. Indeed, we have conducted our analysis with an idealized model where
 353 only three layers are used in the vertical, while ocean surface current feedback is well confined
 354 within the upper 30-50m of the ocean in realistic conditions (Ma et al. 2016). Our results thus
 355 provide a first step in this direction, in the context of QG dynamics, and should be further validated.

356 Comparing the horizontal structures of eddy-mean flow energy transfers, we highlighted the
 357 opposite behaviour between kinetic and potential energy. For kinetic energy, production or de-
 358 struction of MKE through K_{MEC} is larger along the jet while its associated EKE component,
 359 K_{EF} , is larger on the flanks of the jet, an organization largely driven by the horizontal structure of

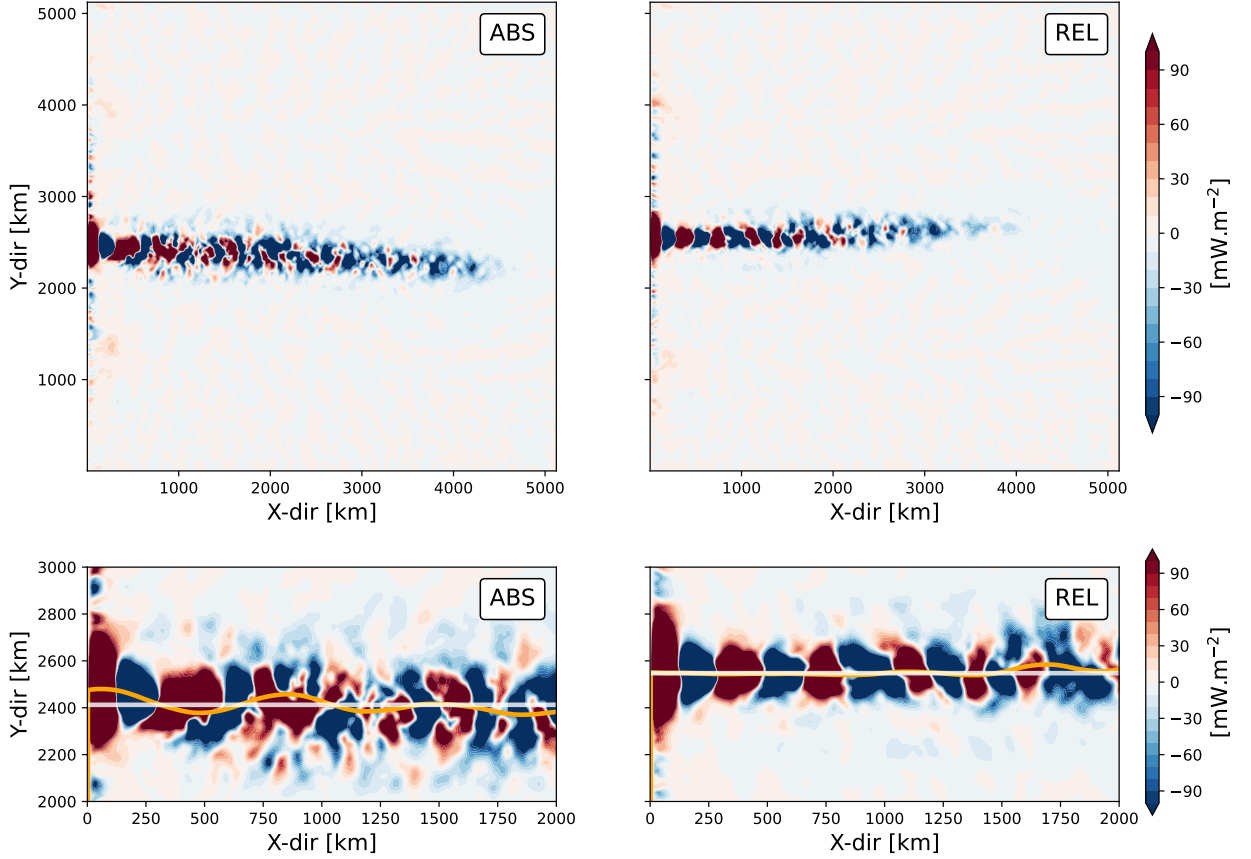


FIG. 8: (Top two panels) Depth integrated contribution of P_{EF} for the absolute (left) and the relative (right) run. Red shading indicate a local source of EPE. (Bottom two panels) A zoom on the jet region showing the spatial organization of P_{EF} relative to the time mean zero mean streamfunction $\bar{\psi}$ in the first layer (orange contour). The white line indicate the meridional position of the zonally averaged time mean zero mean streamfunction in the 2000 km away from the western boundary.

360 the mean flow and that of its gradients, respectively (see Jamet et al. 2022, for broader discussion).
 361 Our results suggest that a similar argument can be made for potential energy but with an opposite
 362 structure, namely that production or destruction of MPE through P_{MEC} is larger on the flanks
 363 of the stream and its associated EPE component, P_{EF} , is larger along the jet. This may well
 364 suggest that similar dynamical constrains, as reported by Jamet et al. (2022), could be relevant to
 365 better understand how the mean flow and the eddy dynamics exchange their energy, thus reach an
 366 energetically balanced state. Given that non-local eddy-mean flow energy transfers as been found
 367 to be of larger magnitude for the potential energy than for the kinetic energy by Chen et al. (2014), it

³⁶⁸ would be of interest to further study such potential dynamical constraints in the context of potential
³⁶⁹ energy.

370 *Acknowledgments.* We thank Lionel Renault for stimulating discussions on this topic, and the
 371 two anonymous reviewers for their very constructive comments. This work was supported by the
 372 French National program LEFE (Les Enveloppes Fluides et l'Environnement).

373 *Data availability statement.* Lorenz Energy Cycles and associated vertically inte-
 374 grated maps and spectral fluxes have been computed with the qgutils python pack-
 375 ages (<https://zenodo.org/badge/latestdoi/612190785>). The Q-GCM model parameters,
 376 along with python scripts used to produce results discussed here are available at
 377 <https://zenodo.org/badge/latestdoi/258128829>.

378 APPENDIX A

379 Lorenz Energy Cycle in quasi-geostrophic models

380 The Lorenz Energy Cycle (LEC), originally formulated for the atmosphere by Lorenz (1955)
 381 and subsequently adapted to the ocean (Harrison and Robinson 1978; Oort et al. 1994), provides
 382 a descriptive understanding of the different energy reservoirs of a Boussinesq, incompressible
 383 fluid (ocean or atmosphere) partitioned into four quantities usually referred to as Mean Potential
 384 Energy and Mean Kinetic Energy (MPE, MKE, respectively) and its Eddy counterpart (EPE, EKE,
 385 respectively). Analysis of the LEC allows to identify leading order energetic contributions for the
 386 ocean circulation, as well as the myriad of interactions between the different reservoirs and the
 387 external forcings (momentum and buoyancy fluxes, boundary contribution in the case of a regional
 388 analysis).

389 The time evolution of the QG Potential Vorticity equation is defined as (ignoring forcing and
 390 dissipation for simplicity)

$$\partial_t q + \mathbf{u}_g \cdot \nabla_h q = 0, \quad (\text{A1})$$

391 with the \mathbf{u}_g the geostrophic velocities and

$$q = \Delta\psi + \beta(y - y_0) + \partial_z \left(\frac{f_0^2}{N^2} \partial_z \psi \right), \quad (\text{A2})$$

392 the QG Potential Vorticity, defined based on the streamfunction $\psi = \frac{p}{\rho_0 f_0}$ where p is pressure, ρ_0
 393 the reference density and f_0 the reference Coriolis frequency used in the β -plane approximation

394 $f = f_0 + \beta(y - y_0)$. Equation (A1) provides a single evolution equation constructed based on
 395 the momentum and the continuity equations for an incompressible, Boussinesq fluid subject to
 396 geostrophic approximations, i.e.

$$\partial_t(\Delta\psi) = -J(\psi, \Delta\psi) + f_0\partial_z w \quad (\text{A3})$$

397 for the momentum equation and

$$f_0\partial_t(\partial_z\psi) = -f_0J(\psi, \partial_z\psi) - N^2w \quad (\text{A4})$$

398 for the buoyancy equation (buoyancy is here defined as $b = f_0\partial_z\psi$), where $J(A, B) = \partial_x A \partial_y B -$
 399 $\partial_x B \partial_y A$ is the Jacobian operator, $\Delta = \nabla^2 = \partial_x^2 + \partial_y^2$ is the Laplacian operator and w are the
 400 ageostrophic, small amplitude vertical velocities. An equation of evolution for the Kinetic Energy

$$KE = \frac{1}{2} (\nabla\psi \cdot \nabla\psi) \quad (\text{A5})$$

401 and for the potential energy

$$PE = \frac{1}{2} \left(\frac{f_0^2}{N^2} (\partial_z\psi)^2 \right) \quad (\text{A6})$$

402 are then obtained by multiplying Eq. (A3) by $-\psi$ and Eq. (A4) by $\frac{f_0}{N^2}\partial_z\psi$, respectively. Volume
 403 integrated kinetic and potential energy equations read

$$\int_{\Omega} \partial_t KE \, dV = \int_{\Omega} \psi J(\psi, \Delta\psi) \, dV - \int_{\Omega} f_0\psi \partial_z w \, dV, \quad (\text{A7})$$

404 and

$$\int_{\Omega} \partial_t PE = - \int_{\Omega} \frac{f_0^2}{N^2} \partial_z\psi J(\psi, \partial_z\psi) \, dV - \int_{\Omega} f_0\partial_z\psi \, w \, dV, \quad (\text{A8})$$

405 where Ω is the full domain.

406 We now introduce the Reynolds decomposition

$$X = \bar{X} + X', \quad (\text{A9})$$

407 with \bar{X} a time averaging. We apply this decomposition to Eq. (A7) and Eq. (A8) to get the Eddy
 408 Kinetic and Potential Energy (EKE= $\overline{KE'}$, EPE= $\overline{PE'}$) and the Mean Kinetic and Potential Energy
 409 (MKE= $\overline{\overline{KE}}$, MPE= $\overline{\overline{PE}}$)

$$\int \partial_t \overline{\overline{KE}} dV = \int \left(\overline{\psi} J(\overline{\psi}, \Delta \overline{\psi}) + \overline{\psi} \overline{J(\psi', \Delta \psi')} - \underbrace{f_0 \overline{\psi} \partial_z \overline{w}}_{=\overline{wb}} \right. \\ \left. - \frac{\delta_E f_0}{2H_2} \overline{\psi} \Delta \overline{\psi} - f_0 \overline{\psi w_{ek}} \right) dV \quad (\text{A10})$$

$$\int \partial_t \overline{KE'} dV = \int \left(\overline{\psi' J(\psi', \Delta \psi')} + \overline{\psi' J(\overline{\psi}, \Delta \psi')} + \overline{\psi' J(\psi', \Delta \psi')} \right. \\ \left. - \underbrace{f_0 \overline{\psi' \partial_z w'}}_{=\overline{w'b'}} - \frac{\delta_E f_0}{2H_2} \overline{\psi' \Delta \psi'} - f_0 \overline{\psi' w'_{ek}} \right) dV \quad (\text{A11})$$

$$\int \partial_t \overline{\overline{PE}} dV = \int \left(-\frac{f_0^2}{N^2} \overline{\partial_z \psi} J(\overline{\psi}, \partial_z \overline{\psi}) - \frac{f_0^2}{N^2} \partial_z \overline{\psi} \overline{J(\psi', \partial_z \psi')} \right. \\ \left. - \underbrace{f_0 \partial_z \overline{\psi} \overline{w}}_{=\overline{wb}} + f_0 \partial_z \overline{\psi} \left(\frac{\Delta T_m w_{ek}}{\Delta T_1} \right) \right) dV \quad (\text{A12})$$

$$\int \partial_t \overline{PE'} dV = \int \left(-\frac{f_0^2}{N^2} \overline{\partial_z \psi'} J(\psi', \partial_z \overline{\psi}) - \frac{f_0^2}{N^2} \partial_z \psi' \overline{J(\overline{\psi}, \partial_z \psi')} - \frac{f_0^2}{N^2} \partial_z \psi' \overline{J(\psi', \partial_z \psi')} \right. \\ \left. - \underbrace{f_0 \partial_z \psi' \overline{w'}}_{=\overline{w'b'}} + f_0 \partial_z \psi' \left(\frac{\Delta T_m w_{ek}}{\Delta T_1} \right)' \right) dV. \quad (\text{A13})$$

410 Dynamical interpretations of the terms in equations Eq. (A10)-(A13) are provided in Table A1.
 411 In this paper, we will focus on the terms of transfers of energy between the four reservoirs, and
 412 analyze their sensitivity to wind stress formulation and their non-locality.

413 APPENDIX B

414 Non-local energy transfers in quasi-geostrophic models

415 Following previous studies (e.g. Harrison and Robinson 1978; Chen et al. 2014), we will refer to
 416 local processes when the energy lost by the mean flow sustains *locally* the growth of perturbations

Reservoir	Mathematical expression	Physical interpretation
MKE	$\overline{\psi J(\overline{\psi}, \Delta\overline{\psi})}$ $\overline{\psi J(\psi', \Delta\psi')}$ $\overline{w\overline{b}}$ $-f_0 \overline{\psi w_{ek}}$	MKE advection energy exchanges with the EKE (K_MEC) energy conversion with the MPE mean wind work
EKE	$\overline{\psi' J(\psi', \Delta\overline{\psi})}$ $\overline{\psi' J(\psi, \Delta\psi')}$ $\overline{w'b'}$ $-f_0 \overline{\psi' w'_{ek}}$	energy exchanges with the MKE (K_EF) EKE advection (by both the mean and the turbulent flow) energy conversion with the EPE turbulent wind work
MPE	$-\frac{1}{N^2} \overline{\overline{b} J(\overline{\psi}, \overline{b})}$ $-\frac{1}{N^2} \overline{\overline{b} J(\psi', b')}$ $-\overline{w\overline{b}}$ $\overline{\overline{b} \left(\frac{\Delta T_m w_{ek}}{\Delta T_1} \right)}$	MPE advection energy exchanges with the EPE (P_MEC) energy conversion with the MKE mean diabatic heating
EPE	$-\frac{1}{N^2} \overline{b' J(\psi', \overline{b})}$ $-\frac{1}{N^2} \overline{b' J(\psi, b')}$ $-\overline{w'b'}$ $\overline{b' \left(\frac{\Delta T_m w_{ek}}{\Delta T_1} \right)'}$	energy exchanges with the MPE (P_EF) EPE advection (by both the mean and the turbulent flow) energy conversion with the EKE turbulent diabatic heating

TABLE A1: Table explaining the physical meaning for each term present in energy equations. Bold text on the right column refers to the shorthands used throughout this paper to refer to eddy-mean flow energy transfers ; they read as **Kinetic Mean-to-Eddy C**onversion (**K_MEC**) and **Kinetic Eddy Flux** (**K_EF**) for kinetic energy, and similar for potential energy with **P** in place of **K**. Although we abusively refer to a *conversion* of energy in the shorthand MEC, this choice is made to keep with the notation proposed by Jamet et al. (2021) and Jamet et al. (2022). Buoyancy b is defined here as $b = f_0 \partial_z \psi$.

417 (or vice versa in the case of backscattering). If the energy lost by the mean flow at one location
418 does not sustain the growth of eddies at that location but is exported away, we will refer to it as
419 *non-local* processes. This can be formally understood as the degree of compensation between the
420 two terms of eddy-mean flow interaction in both the mean and eddy energy equations, which are
421 not mathematically the same but are linked through the divergence of a turbulent flux of eddy-mean
422 flow interaction term. For the case of the potential energy, this reads

$$\underbrace{\overline{\overline{b} J(\psi', b')}}_A = \underbrace{\overline{J(\psi', \overline{b} b')}}_B - \underbrace{\overline{b' J(\psi', \overline{b})}}_C \quad (\text{B1})$$

423 where A appears in the MPE equation, C appears in the EPE equation and B is the *non-local*
424 term. The degree of locality can be estimated based on the magnitude of the divergent term
425 $(J(\psi', \overline{bb'}))$: transfers are local when this term is small, and non-local when it is leading order.
426 A similar derivation can be made for the kinetic energy, leading to similar conclusions. We note,
427 however, that when using the vorticity-stream function form of the QG equations, as in the present
428 manuscript, this derivation involves several integration by part. An alternative would be to use
429 the momentum-buoyancy form of QG equations, as in, e.g., Rouillet et al. (2012), but we have not
430 considered it here since our focus is on potential energy. We note that integrated over the full
431 domain subject to no flux boundary conditions, these *non-local* terms are identically zero and do
432 not contribute in the LEC of Fig. 1 and discussed in Section 3.

433 Hereafter we will work with depth integrated energy exchanges. The conversion from potential
434 to kinetic energy (or vice versa) is then exact and expressed as wb . This can be seen by integrating
435 by part (on the vertical) the last term on the RHS of the KE equation Eq. (A7):

$$\int f_0 \psi \partial_z w \, dz = [f_0 \partial_z (\psi w)]_{z=H}^{z=0} - \int w f_0 \partial_z \psi \, dz = - \int w b \, dz \quad (\text{B2})$$

436 with buoyancy $b = f_0 \partial_z \psi$, and where homogeneous surface and bottom (i.e. $w|_{z=\eta, z=H} = b|_{z=\eta, z=H} =$
437 0) boundary conditions have been considered for the divergent term. We exactly recover the
438 production term for the PE equation Eq. (A8).

439 APPENDIX C

440 Spectral Analysis

441 Finally, we will evaluate the wavenumber domain spectral distribution of energy reservoirs as well
442 as their associated spectral energy fluxes. The different terms derived in the physical space in
443 Appendix A and Appendix B are transposed in spectral space as follow. We will first consider the
444 kinetic energy by considering the material derivative of relative vorticity. As such, we will not
445 write the terms representing the energy losses and gains because they can be treated just as will
446 be treated the advection term in the following demonstration. An expression with all the terms

447 written will be mentioned later.

$$\frac{D\zeta}{Dt} = \frac{\partial\zeta}{\partial t} + u\nabla\zeta. \quad (\text{C1})$$

448 We first carry out a discrete Fourier transform on our equation, noting $A = u\nabla\zeta$:

$$\frac{\partial\zeta}{\partial t} + A = \sum_{\vec{k}} \frac{\partial}{\partial t} \widehat{\zeta}_k e^{i\vec{k}\cdot\vec{x}} + \sum_{\vec{k}} \widehat{A}_k e^{i\vec{k}\cdot\vec{x}}. \quad (\text{C2})$$

449 To obtain the time derivative of the kinetic energy at one wavenumber, we multiply the above
 450 equation by the complex conjugate of the Discrete Fourier transform of ψ at the wavenumber r
 451 (similar to what we did to go from Eq. (A3) to Eq. (A7)):

$$\psi \left[\sum_{\vec{k}} \frac{\partial}{\partial t} \widehat{\zeta}_k e^{i\vec{k}\cdot\vec{x}} + \sum_{\vec{k}} \widehat{A}_k e^{i\vec{k}\cdot\vec{x}} \right] = \widehat{\psi}_{k_r}^* e^{-i\vec{k}_r\cdot\vec{x}} \left[\sum_{\vec{k}} \frac{\partial}{\partial t} \widehat{\zeta}_k e^{i\vec{k}\cdot\vec{x}} + \sum_{\vec{k}} \widehat{A}_k e^{i\vec{k}\cdot\vec{x}} \right]. \quad (\text{C3})$$

452 Since Fourier modes are orthogonal, only remains the following:

$$\widehat{\psi}_{k_r}^* e^{-i\vec{k}_r\cdot\vec{x}} \left[\sum_{\vec{k}} \frac{\partial}{\partial t} \widehat{\zeta}_k e^{i\vec{k}\cdot\vec{x}} + \sum_{\vec{k}} \widehat{A}_k e^{i\vec{k}\cdot\vec{x}} \right] = \widehat{\psi}_{k_r}^* \frac{\partial}{\partial t} \widehat{\zeta}_{k_r} + \widehat{\psi}_{k_r}^* \widehat{A}_{k_r}. \quad (\text{C4})$$

453 The first term on the right hand side accounts for the time derivative of the kinetic energy at
 454 one wavenumber. We note that from equation Eq. (C4), we obtain a 2D spectrum because the
 455 wavenumbers are divided into a zonal and a meridional part. Before further computation, an
 456 azimuthal average is performed on the 2D spectrum to obtain a 1D spectrum, the 1D wavenumbers
 457 obtained thus correspond to the radial wavenumbers of the 2D spectrum: from $\vec{k}_r = (k_r, l_r)$, we
 458 obtain $r = k_r^2 + l_r^2$.

459 Now including the forcing and dissipation term initially appearing in the relative vorticity
 460 equation, we obtain:

$$\frac{\partial \widehat{KE}_r}{\partial t} = -\widehat{\psi}_r^* \widehat{A}_r - \underbrace{f_0 \widehat{\psi}_r^* \frac{\partial \widehat{w}_r}{\partial z}}_{\widehat{w}^* \widehat{b}} + \widehat{\psi}_r^* \widehat{F}_{w_r} + \widehat{\psi}_r^* \widehat{D}_r. \quad (\text{C5})$$

461 The interest behind this demonstration is to obtain an expression for the spectral fluxes, meaning
 462 at which wavenumbers energy from a reservoir is leaked or inserted due to a certain term. For the
 463 specific case of potential-to-kinetic energy conversion term wb , it is of interest to further consider
 464 the spectral estimate of w which, in QG, can be expressed through the density equation as:

$$w = \frac{1}{N^2} (\partial_t + \mathbf{u}_g \cdot \nabla_h) \left(\underbrace{f_0 \partial_z \psi}_{=b} \right). \quad (\text{C6})$$

465 The advective component of w can then be written in terms of buoyancy $b = f_0 \partial_z \psi$ and stream
 466 function ψ , as

$$w^{(\text{adv})} = \frac{1}{N^2} J(\psi, b), \quad (\text{C7})$$

467 with $J(A, B) = \partial_x A \partial_y B - \partial_x B \partial_y A$ the Jacobian operator. Expressing the streamfunction and the
 468 buoyancy in Fourier modes, i.e. $\psi = \sum_{\mathbf{p}} \widehat{\psi}(\mathbf{p}, t) e^{i\mathbf{p} \cdot \mathbf{x}}$ and $b = \sum_{\mathbf{q}} \widehat{b}(\mathbf{q}, t) e^{i\mathbf{q} \cdot \mathbf{x}}$, we can then express
 469 the (conjugate of) Fourier transform of w as:

$$\begin{aligned} \widehat{w}^* &= \frac{1}{N^2} \overline{J(\psi, b)}^* \\ &= \frac{1}{N^2} \left(\sum_{\mathbf{p}} p^x \widehat{\psi}(\mathbf{p}, t) e^{i\mathbf{p} \cdot \mathbf{x}} \sum_{\mathbf{q}} q^y \widehat{b}(\mathbf{q}, t) e^{i\mathbf{q} \cdot \mathbf{x}} - \sum_{\mathbf{p}} p^y \widehat{\psi}(\mathbf{p}, t) e^{i\mathbf{p} \cdot \mathbf{x}} \sum_{\mathbf{q}} q^x \widehat{b}(\mathbf{q}, t) e^{i\mathbf{q} \cdot \mathbf{x}} \right)^* \\ &= \frac{1}{N^2} \int \left(\sum_{\mathbf{p}, \mathbf{q}} (p^x q^y - p^y q^x) \widehat{\psi} \widehat{b} e^{-i(\mathbf{p} + \mathbf{q}) \cdot \mathbf{x}} \right) e^{i\mathbf{k} \cdot \mathbf{x}} d\mathbf{x} \\ &= \frac{1}{N^2} \sum_{\mathbf{p}, \mathbf{q}} A(\mathbf{p}, \mathbf{q}, \mathbf{k}) \widehat{\psi} \widehat{b}, \end{aligned} \quad (\text{C8})$$

470 with $A(\mathbf{p}, \mathbf{q}, \mathbf{k}) = (p^x q^y - p^y q^x) \delta(\mathbf{k} - \mathbf{p} - \mathbf{q})$ an 'interaction coefficient' similar to what can be
 471 derived for the advective term in QG (See Vallis (2006)). Upon multiplication by \widehat{b} to obtain a
 472 spectral estimate of wb , we can then identify a cross-scale KE transfer. Azimutally averaging
 473 the obtained two-dimensional power spectral provides spectral estimates of energy conversion
 474 repartition across different scales. However, the resulting spectra is hardly readable because
 475 of steep variations along small range of wavenumber, and it is common to instead perform a
 476 wavenumber integration assuming that the flux vanishes at the highest wavenumber (Capet et al.

477 2008b; Arbic et al. 2013), such that

$$\Pi_{wb}(\mathbf{k}) = \int_{\mathbf{k}}^{\infty} \widehat{w}^* \widehat{b} d\mathbf{k}. \quad (\text{C9})$$

478 Formally, this should be interpreted as the net contribution of energy fluxes from smallest resolved
 479 scales to the scale associated with wavenumber \mathbf{k} . Previously, a positive value of wb meant a
 480 conversion from potential to kinetic energy, now it is represented by a negative slope.

481 APPENDIX D

482 Effects of relative wind stress on wind work

483 We briefly review here the demonstration that relative wind stress formulation leads to a sign
 484 definite contribution in wind work. This demonstration is largely inspired by that of Zhai and
 485 Greatbatch (2007). We note, however, that no assumptions of scale, amplitude nor direction of
 486 atmospheric winds and ocean surface currents are made here, as opposed to, e.g. Duhaut and
 487 Straub (2006).

488 Consider the wind work WW_1 and WW_2 , defined as

$$WW^{(1,2)} = \boldsymbol{\tau}^{(1,2)} \cdot \rho_0 \mathbf{u}_o, \quad (\text{D1})$$

489 with the wind stress $\boldsymbol{\tau}^{(1)}$ defined with an *absolute* formulation (Eq. (2)) and $\boldsymbol{\tau}^{(2)}$ defined with a
 490 *relative* formulation (Eq. (1)). We want to evaluate the sign of the energy changes induced by the
 491 ocean current feedback. For this, consider the change in wind work (ignoring potential changes in
 492 drag coefficients C_d and atmospheric wind \mathbf{u}_a)

$$\frac{\Delta WW}{\rho_0 \rho_a C_d} = \frac{WW^{(2)} - WW^{(1)}}{\rho_0 \rho_a C_d} = \underbrace{(|\mathbf{u}_a - \mathbf{u}_o| - |\mathbf{u}_a|) \mathbf{u}_a \cdot \mathbf{u}_o}_A - \underbrace{|\mathbf{u}_a - \mathbf{u}_o| \mathbf{u}_o \cdot \mathbf{u}_o}_B. \quad (\text{D2})$$

493 One can easily show that $B > 0$ for all conditions (i.e. both $|\mathbf{u}_a - \mathbf{u}_o|$ and $\mathbf{u}_o \cdot \mathbf{u}_o$ are positive
 494 definite), thus it represents a sink of energy ($-B < 0$). However, the sign definiteness of A is less
 495 obvious, and two scenarios should be considered depending on the sign of $\mathbf{u}_a \cdot \mathbf{u}_o$.

496 We first consider the case when $\mathbf{u}_a \cdot \mathbf{u}_o < 0$, which would imply that ($|\mathbf{u}_a - \mathbf{u}_o| > |\mathbf{u}_a|$) for A to
 497 be sign definite and negative (i.e. a sink of energy). Squaring the later inequality leads to:

$$|\mathbf{u}_a|^2 < |\mathbf{u}_a - \mathbf{u}_o|^2 \quad (\text{D3a})$$

$$\mathbf{u}_a \cdot \mathbf{u}_a < (\mathbf{u}_a - \mathbf{u}_o) \cdot (\mathbf{u}_a - \mathbf{u}_o) \quad (\text{D3b})$$

$$\mathbf{u}_a \cdot \mathbf{u}_o < \frac{1}{2} \mathbf{u}_o \cdot \mathbf{u}_o. \quad (\text{D3c})$$

498 Inequality (D3c) is valid for $\mathbf{u}_a \cdot \mathbf{u}_o < 0$ (our current condition) since surface kinetic energy $\frac{1}{2} \mathbf{u}_o \cdot \mathbf{u}_o$
 499 is defined positive.

500 However, if $\mathbf{u}_a \cdot \mathbf{u}_o > 0$, the condition of having sign definite (i.e. a sink of energy) for A requires

$$|\mathbf{u}_a| > |\mathbf{u}_a - \mathbf{u}_o| \quad (\text{D4})$$

501 leading to (once squared):

$$\mathbf{u}_a \cdot \mathbf{u}_o > \frac{1}{2} \mathbf{u}_o \cdot \mathbf{u}_o. \quad (\text{D5})$$

502 Thus, in the case where $0 < \mathbf{u}_a \cdot \mathbf{u}_o < \frac{1}{2} \mathbf{u}_o \cdot \mathbf{u}_o$, the contribution of A is a source of kinetic energy for
 503 the ocean. This is satisfied only in specific conditions, i.e. when wind and currents are in the same
 504 direction (defined on a $[-\pi/2; \pi/2]$ orientation centered with \mathbf{u}_a or \mathbf{u}_o), the *relative* wind work will
 505 induce a source of kinetic energy for the ocean surface current if the dot product of atmospheric
 506 winds with oceanic surface currents is weaker than the kinetic energy of the ocean surface currents.
 507 This can be associated with either weak wind conditions, or wind conditions nearly orthogonal to
 508 the ocean surface currents. Nonetheless, although A is not always sign definite and can contribute
 509 positively to ocean kinetic energy, such positive contribution will remain weaker than that of B
 510 such that the overall wind work difference induced by ocean surface current will always act as a
 511 sink of energy for the ocean. This last statement has been verified numerically (not shown).

512 References

513 Arbic, B. K., K. L. Polzin, R. B. Scott, J. G. Richman, and J. F. Shriver, 2013: On eddy viscosity,
 514 energy cascades, and the horizontal resolution of gridded satellite altimeter products. *J. Phys.*
 515 *Oceanogr.*, **43** (2), 283–300.

- 516 Capet, X., J. C. McWilliams, M. J. Molemaker, and A. Shchepetkin, 2008a: Mesoscale to sub-
517 mesoscale transition in the California Current System. Part I: Flow structure, eddy flux, and
518 observational tests. *J. Phys. Oceanogr.*, **38** (1), 29–43.
- 519 Capet, X., J. C. McWilliams, M. J. Molemaker, and A. F. Shchepetkin, 2008b: Mesoscale to
520 submesoscale transition in the California Current System. Part III: Energy balance and flux. *J.*
521 *Phys. Oceanogr.*, **38** (10), 2256–2269.
- 522 Chen, R., G. R. Flierl, and C. Wunsch, 2014: A description of local and nonlocal eddy–mean flow
523 interaction in a global eddy-permitting state estimate. *J. Phys. Oceanogr.*, **44** (9), 2336–2352.
- 524 Dawe, J. T., and L. Thompson, 2006: Effect of ocean surface currents on wind stress, heat flux,
525 and wind power input to the ocean. *Geophys. Res. Lett.*, **33** (9).
- 526 Deremble, B., T. Uchida, W. K. Dewar, and R. Samelson, 2023: Eddy-mean flow interaction with
527 a multiple scale quasi geostrophic model. *J. Adv. Model. Earth Syst.*, **15** (10), e2022MS003 572,
528 <https://doi.org/10.1029/2022MS003572>.
- 529 Dewar, W. K., and G. R. Flierl, 1987: Some effects of the wind on rings. *J. Phys. Oceanogr.*,
530 **17** (10), 1653–1667.
- 531 Duhaut, T. H., and D. N. Straub, 2006: Wind stress dependence on ocean surface velocity:
532 Implications for mechanical energy input to ocean circulation. *J. Phys. Oceanogr.*, **36** (2), 202–
533 211.
- 534 Gaube, P., D. B. Chelton, R. M. Samelson, M. G. Schlax, and L. W. O’Neill, 2015: Satellite
535 observations of mesoscale eddy-induced ekman pumping. *J. Phys. Oceanogr.*, **45**, 104–132,
536 <https://doi.org/10.1175/JPO-D-14-0032.1>.
- 537 Harrison, D., and A. Robinson, 1978: Energy analysis of open regions of turbulent flows—Mean
538 eddy energetics of a numerical ocean circulation experiment. *Dyn. Atmos. Oceans*, **2** (2), 185–
539 211.
- 540 Hogg, A., J. Blundell, W. Dewar, and P. Killworth, 2014: Formulation and users’ guide for Q-GCM.
541 URL <http://q-gcm.org/downloads.html>.

- 542 Hogg, A. M. C., W. K. Dewar, P. D. Killworth, and J. R. Blundell, 2006: Decadal variability of the
543 midlatitude climate system driven by the ocean circulation. *J. Clim.*, **19** (7), 1149–1166.
- 544 Jamet, Q., B. Deremble, N. Wienders, T. Uchida, and W. Dewar, 2021: On Wind-driven Energetics
545 of Subtropical Gyres. *Journal of Advances in Modeling Earth Systems*, e2020MS002329.
- 546 Jamet, Q., S. Leroux, W. K. Dewar, T. Penduff, J. Le Sommer, J.-M. Molines, and J. Gula, 2022:
547 Non-local eddy-mean kinetic energy transfers in submesoscale-permitting ensemble simulations.
548 *Manuscript in preparation for submission, ..--.*
- 549 Jullien, S., S. Masson, V. Oerder, G. Samson, F. Colas, and L. Renault, 2020: Impact of Ocean–
550 Atmosphere Current Feedback on Ocean Mesoscale Activity: Regional Variations and Sensitiv-
551 ity to Model Resolution. *J. Clim.*, **33** (7), 2585–2602.
- 552 Kang, D., and E. N. Curchitser, 2015: Energetics of eddy–mean flow interactions in the Gulf
553 Stream region. *J. Phys. Oceanogr.*, **45** (4), 1103–1120.
- 554 Lorenz, E. N., 1955: Available potential energy and the maintenance of the general circulation.
555 *Tellus*, **7** (2), 157–167.
- 556 Ma, X., and Coauthors, 2016: Western boundary currents regulated by interaction between ocean
557 eddies and the atmosphere. *Nature*, **535** (7613), 533–537.
- 558 Martin, P. E., B. K. Arbic, A. McC. Hogg, A. E. Kiss, J. R. Munroe, and J. R. Blundell, 2020:
559 Frequency-Domain Analysis of the Energy Budget in an Idealized Coupled Ocean–Atmosphere
560 Model. *Journal of Climate*, **33** (2), 707–726.
- 561 Matsuta, T., and Y. Masumoto, 2021: Modified view of energy budget diagram and its application
562 to the kuroshio extension region. *J. Phys. Oceanogr.*, **51** (4), 1163–1175.
- 563 Matsuta, T., and Y. Masumoto, 2023: Energetics of the antarctic circumpolar current. part i: The
564 lorenz energy cycle and the vertical energy redistribution. *J. Phys. Oceanogr.*, **53** (6), 1467–1484.
- 565 McCaffrey, K., B. Fox-Kemper, and G. Forget, 2015: Estimates of ocean macroturbulence: Struc-
566 ture function and spectral slope from Argo profiling floats. *J. Phys. Oceanogr.*, **45** (7), 1773–1793.
- 567 Murakami, S., 2011: Atmospheric local energetics and energy interactions between mean and eddy
568 fields. part i: Theory. *J. Atmos. Sci.*, **68** (4), 760–768.

- 569 Oort, A. H., L. A. Anderson, and J. P. Peixoto, 1994: Estimates of the energy cycle of the oceans.
570 *Journal of Geophysical Research: Oceans*, **99 (C4)**, 7665–7688.
- 571 Pacanowski, R., 1987: Effect of equatorial currents on surface stress. *J. Phys. Oceanogr.*, **17 (6)**,
572 833–838.
- 573 Renault, L., P. Marchesiello, S. Masson, and J. C. McWilliams, 2019: Remarkable control of
574 western boundary currents by eddy killing, a mechanical air-sea coupling process. *Geophys.*
575 *Res. Lett.*, **46 (5)**, 2743–2751.
- 576 Renault, L., M. J. Molemaker, J. Gula, S. Masson, and J. C. McWilliams, 2016: Control and
577 stabilization of the gulf stream by oceanic current interaction with the atmosphere. *J. Phys.*
578 *Oceanogr.*, **46 (11)**, 3439–3453.
- 579 Roulet, G., J. C. McWilliams, X. Capet, and M. J. Molemaker, 2012: Properties of steady
580 geostrophic turbulence with isopycnal outcropping. *J. Phys. Oceanogr.*, **42 (1)**, 18–38.
- 581 Seo, H., and Coauthors, 2023: Ocean mesoscale and frontal-scale ocean–atmosphere interactions
582 and influence on large-scale climate: A review. *J. Clim.*, **36 (7)**, 1981–2013.
- 583 Song, H., J. Marshall, D. J. McGillicuddy Jr, and H. Seo, 2020: Impact of current-wind interaction
584 on vertical processes in the southern ocean. *Journal of Geophysical Research: Oceans*, **125 (4)**,
585 e2020JC016046.
- 586 Uchida, T., B. Deremble, and S. Popinet, 2022: Deterministic model of the eddy dynamics for a
587 midlatitude ocean model. *Journal of Physical Oceanography*, **52 (6)**, 1133–1154.
- 588 Vallis, G. K., 2006: *Atmospheric and oceanic fluid dynamics: fundamentals and large-scale*
589 *circulation*. Cambridge University Press.
- 590 Waterman, S., and S. R. Jayne, 2011: Eddy-mean flow interactions in the along-stream development
591 of a western boundary current jet: An idealized model study. *J. Phys. Oceanogr.*, **41 (4)**, 682–707.
- 592 Zhai, X., and R. J. Greatbatch, 2007: Wind work in a model of the northwest atlantic ocean.
593 *Geophys. Res. Lett.*, **34 (4)**.

594 Zhu, Y., Y. Li, Y. Yang, and F. Wang, 2023: The role of eddy-wind interaction in the eddy kinetic
595 energy budget of the agulhas retroflection region. *Environmental Research Letters*, **18** (10),
596 104 032.